OPEN ACCESS
JOURNAL OF ADVANCED DIELECTRICS
Vol. 12, No. 4 (2022) 2244002 (6 pages)

DOI: 10.1142/S2010135X22440027

Phase-field study of crystallographic texturing in piezoelectric polycrystals

Meixin Wang*, Tian Xia* and Liwei D. Geng†
Department of Materials Science and Engineering
Sichuan University-Pittsburgh Institute, Sichuan University
Chengdu, Sichuan 610065, P. R. China
†liwei.geng@scupi.cn

Received 1 July 2022; Revised 19 July 2022; Accepted 31 July 2022; Published 18 August 2022

Crystallographic texturing enables the design of piezoelectric polycrystals that outperform traditional random polycrystals by exhibiting outstanding piezoelectric properties. In this work, phase-field modeling and computer simulation were employed to study the effect of crystallographic texture on the piezoelectric properties of ferroelectric polycrystals at the domain level. Domain evolutions for single crystal, random polycrystal, and textured polycrystal are systematically simulated. The simulations reveal that the [001]-textured polycrystal can fully exploit the intrinsic anisotropic properties of piezoelectric materials by exhibiting a piezoelectric coefficient that is as large as that of single crystal while being much larger than that of random polycrystal. To better understand the mechanism of piezoelectricity enhancement by crystallographic texturing, a theoretical analysis based on Landau theory is provided. In comparison with random polycrystal, the textured polycrystal manifests a flatter energy landscape and thus possesses a higher piezoelectric coefficient.

Keywords: Phase-field modeling; piezoelectric polycrystal; crystallographic texture; textured polycrystal.

1. Introduction

Piezoelectric materials find widespread use in the electronic, communication, sensing, imaging, and electromechanical systems.[1–3] In particular, high energy density and ease of miniaturization can further lead to the emergence of new piezoelectric technologies like energy harvesters for the Internet of Things (IoT) devices.[3] As one of the most essential factors in piezoelectric materials, piezoelectric coefficient indicates the magnitude of strain in response to applied electric field or voltage in response to applied mechanical stress. To achieve a large strain or voltage response, high piezoelectricity is required.

Piezoelectric ceramic materials are usually polycrystals with random grain orientations and hence exhibit isotropic macroscopic properties. For single crystals, the piezoelectric properties usually manifest a strong intrinsic anisotropy, so a certain orientation may exhibit better piezoelectric properties than the others. For example, the longitudinal piezoelectric strain/charge coefficient, d_{33}, is up to 2820 pC·N^{-1} in [001]-oriented rhombohedral $Pb[(Mg_{1/3}Nb_{2/3})_{1-x}Ti_x]O_3$ (PMN–PT) single crystals, which is nearly 15 times larger than that of d_{33} (190 pC·N^{-1}) along the [111]-direction.[4] In order to exploit the intrinsic anisotropic properties of the materials, single crystals are desired which, however, are usually expensive or difficult to fabricate. The practical application of single crystals is often limited by their relatively higher cost, time-consuming synthesis process, as well as composition inhomogeneity due to incongruent melting issues. Therefore, it is the piezoelectric polycrystalline ceramics with random grain orientations, rather than the single crystals, that are most widely used in applications based on piezoelectric materials. Nevertheless, the random grain orientations just exhibit averaged piezoelectric properties which are usually not as good as the properties exhibited by single crystals.

One approach to exploit the intrinsic anisotropic properties of piezoelectric materials is crystallographic texturing, and extensive efforts have been made towards developing textured polycrystalline piezoelectric ceramics. Crystallographic texture refers to the collective distribution of grain orientations towards a preferred orientation in a polycrystal.[5] Textured polycrystals offer a better cost–performance ratio for achieving anisotropic properties. Enhanced piezoelectric properties in various textured piezoelectric ceramics have been reported.[6–14] Recently, an ultrahigh longitudinal piezoelectric coefficient, $d_{33} \sim 2000$ pC·N^{-1}, was reported in [001]-textured PMN–PT ceramics, which is about two–five times higher than that of the random ceramics.[15] Therefore, textured piezoelectric polycrystals are of technological importance for material applications. Understanding the effect of grain texture on piezoelectricity and the underlying mechanism in textured piezoelectric polycrystals is an important topic.

In this work, phase-field modeling and computer simulation were employed to study the effect of crystallographic

*These authors contributed equally to this work.

texture on the piezoelectric properties of ferroelectric polycrystals at the domain level. Domain evolutions or polarization distributions for single crystals, random polycrystals, and textured polycrystals are systematically simulated. To better understand the mechanism of piezoelectricity enhancement by crystallographic texturing, a theoretical analysis based on Landau theory is provided.

2. Phase-Field Model of Ferroelectric Polycrystal

Phase-field model of ferroelectrics is adopted to perform the simulation study. The grain structure of a polycrystal is characterized by a grain rotation matrix field $\mathbf{R}(\mathbf{r})$ that describes the geometry (size, shape, and location) and crystallographic orientation (texture) of individual grains. The state of such a ferroelectric polycrystal is described by a polarization vector field $\mathbf{P}(\mathbf{r})$, and the total system free energy under externally applied electric field $\mathbf{E}^{ex}$ is[16–19]

$$F = \int d^3r \left[f\left(R_{ij}P_j\right) + \frac{\beta}{2}\frac{\partial P_i}{\partial r_j}\frac{\partial P_i}{\partial r_j} - E_k^{ex}P_k \right] + \frac{1}{2}\int \frac{d^3k}{(2\pi)^3}\left[\frac{n_i n_j}{\varepsilon_0}\tilde{P}_i\tilde{P}_j^* + K_{ijkl}\tilde{\varepsilon}_{ij}^0\tilde{\varepsilon}_{kl}^{0*} \right], \quad (1)$$

where

$$\begin{aligned} f(\mathbf{P}) &= \alpha_1\left(P_1^2+P_2^2+P_3^2\right) + \alpha_{11}\left(P_1^4+P_2^4+P_3^4\right) \\ &+ \alpha_{12}\left(P_1^2P_2^2+P_2^2P_3^2+P_3^2P_1^2\right) + \alpha_{111}\left(P_1^6+P_2^6+P_3^6\right) \\ &+ \alpha_{112}\left[P_1^4\left(P_2^2+P_3^2\right)+P_2^4\left(P_3^2+P_1^2\right)+P_3^4\left(P_1^2+P_2^2\right)\right] \\ &+ \alpha_{123}P_1^2P_2^2P_3^2 \end{aligned} \quad (2)$$

is the Landau–Ginzburg–Devonshire (LGD) free energy function of ferroelectric single crystal.[20] It is worth noting that $\mathbf{P}(\mathbf{r})$ in Eq. (1) is defined in a global coordinate system attached to the polycrystal, while $\mathbf{P}(\mathbf{r})$ in Eq. (2) is defined in a local coordinate system aligned with the ⟨100⟩ lattice axes of a ferroelectric single crystal, and the operation $R_{ij}P_j$ in $f(R_{ij}P_j)$ in Eq. (1) transforms $\mathbf{P}(\mathbf{r})$ from the global sample system to the local lattice system in each grain. The gradient term characterizes energy contribution from polarization gradient in domain wall regions, where β is the gradient coefficient. The $\mathbf{k}$-space integral terms characterize the domain configuration-dependent electrostatic energy of polarization distribution $\mathbf{P}(\mathbf{r})$ and elastostatic energy of misfit strain distribution $\boldsymbol{\varepsilon}^0(\mathbf{r})$, where ε_0 is the permittivity of free space, $\tilde{\mathbf{P}}(\mathbf{k})$ and $\tilde{\boldsymbol{\mu}}(\mathbf{k})$ are the Fourier transforms of the respective field variables $\mathbf{P}(\mathbf{r})$ and $\boldsymbol{\varepsilon}(\mathbf{r})$. The spontaneous electrostrictive strain ε is coupled to polarization $\mathbf{P}$ through the electrostriction coefficient tensor Q_{ijkl}, $\varepsilon_{ij} = Q_{ijkl}P_kP_l$. $K_{ijkl} = C_{ijkl} - n_mC_{ijmn}\Omega_{np}C_{klpq}n_q$, $\Omega_{ik} = (C_{ijkl}n_jn_l)^{-1}$, C_{ijkl} is the elastic modulus tensor, and $\mathbf{n} = \mathbf{k}/k$. The spatial–temporal evolution of the polarization $\mathbf{P}(\mathbf{r},t)$ in response to varying electric field $\mathbf{E}^{ex}(t)$ is characterized by the time-dependent Ginzburg–Landau equation[16–19]

$$\frac{\partial \mathbf{P}(\mathbf{r},t)}{\partial t} = -L\frac{\delta F}{\delta \mathbf{P}(\mathbf{r},t)}, \quad (3)$$

where L is the kinetic coefficient. In this study, we adopted PMN–30PT as the piezoelectric material, which is in rhombohedral phase at room temperature. For the textured piezoelectric polycrystals, the templates are made of single crystal $BaTiO_3$. Thus, the following LGD coefficients are adopted in the phase-field simulations: $\alpha_1 = 0.745(T + 160.45) \times 10^5$ m/F, $\alpha_{11} = -0.50 \times 10^8$ m^5/C^{2}F, $\alpha_{12} = -0.5125 \times 10^8$ m^5/C^{2}F, $\alpha_{111} = 0.5567 \times 10^9$ m^9/C^{4}F, $\alpha_{112} = 1.333 \times 10^9$ m^9/C^{4}F, and $\alpha_{123} = 0.24 \times 10^9$ m^9/C^{4}F for the PMN–30PT matrix[21]; $\alpha_1 = 3.34(T-381) \times 10^5$ m/F, $\alpha_{11} = (4.69(T - 393) \times 10^6 - 2.02 \times 10^8)$ m^5/C^{2}F, $\alpha_{12} = 3.23\times10^8$ m^5/C^{2}F, $\alpha_{111} = (-5.52(T - 393) \times 10^7 + 2.76 \times 10^9)$ m^9/C^{4}F, $\alpha_{112} = 4.47 \times 10^9$ m^9/C^{4}F, and $\alpha_{123} = 4.91 \times 10^9$ m^9/C^{4}F for the $BaTiO_3$ templates.[22] T is the temperature in K. The electrostrictive coefficients are $Q_{11} = 0.055$ m^4·C^{-2}, $Q_{12} = -0.023$ m^4·C^{-2}, and $Q_{44} = 0.0315$ m^4·C^{-2}.

3. Computational Results and Discussion

Under the texturing treatment, the grains are able to align with each other along a specific crystallographic orientation. Such an orientation is usually selected to maximize the piezoelectric performance, so that the design of polycrystalline ceramics can outperform traditional ceramics. Figure 1 schematically illustrates the distributions of grain orientations in random and textured polycrystals. Directions labeled with square brackets, such as [100] and [010], are defined in the "crystallographic coordinate". For random polycrystals, all the orientations are randomly distributed, i.e., the orientations are allowed to rotate around all the three axes. For the [001]-textured polycrystal, however, the orientations are only allowed to rotate around the [001] axis, i.e., all the grains are aligned with each other along the [001] crystallographic axis with the other two crystallographic axes ([010] and [100]) being distributed randomly.

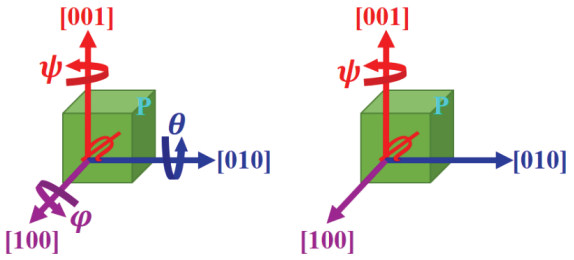

(a) Random (b) [001]-Textured

Fig. 1. Schematic diagram of grain orientation distributions in (a) random and (b) [001]-textured polycrystals. Directions labeled with square brackets are defined in the "crystallographic coordinate".

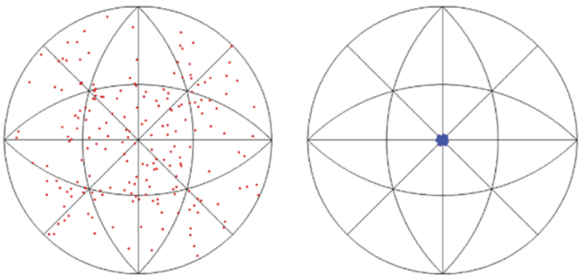

(a) Random (90°) (b) Textured (5°)

Fig. 2. Stereographic projections of (001) plane orientation distributions in representative uniaxial [001]-textured polycrystals: (a) random ($\theta = 90°$) and (b) textured ($\theta = 5°$). The [001] axes of grains are randomly distributed within the solid angle of a cone with half apex angle θ, which measures the degree of uniaxial texture.

In this work, uniaxial [001] texture is considered, which is important for piezoelectric ceramics and can be achieved by templated grain growth technique.[10,23] The grain orientations are randomly generated with their [001] axes distributed within the solid angle of a cone with half apex angle θ, which measures the degree of uniaxial texture, i.e., the smaller the θ, the higher the degree of texture, while the [100] and [010] axes are randomly oriented around the [001] axis of individual grains. Figure 2 shows the stereographic projections of the (001) plane orientation distributions in two representative uniaxial [001]-textured polycrystals, namely, random ($\theta = 90°$) and highly textured ($\theta = 5°$). This stereographic projection diagram is an intuitive way to evaluate the texturing degree.

In this computational study, the orientations, shapes, and sizes of the grains in the polycrystals are separately controlled by using the grain rotation matrix field $\mathbf{R}(\mathbf{r})$, as described in Eq. (1). To investigate the effects of grain texturing, phase-field simulations for three representative microstructures, namely, single crystal, random polycrystal, and textured polycrystal, were performed, as shown in Figs. 3–5, respectively. Figure 1 shows the simulated polarization distribution of single crystal PMN–PT after electrical poling treatment along the [001]-direction. Since the piezoelectric material PMN–PT we adopted in this study is in rhombohedral phase at room temperature, there are eight equivalent ⟨111⟩-directions for those spontaneous polarizations. Before the electrical poling treatment, the eight directions usually emerge with equal probabilities so that the net polarization vanishes. According to the general rule,[24,25] $d_{33} = 2Q_{33}P_r\varepsilon_{33}$, where Q_{33} is the electrostrictive coefficient, P_r is the remanent polarization, and ε_{33} is the dielectric permittivity, the piezoelectricity is negligible for unpoled ferroelectrics due to the zero net polarization. Upon electrical poling along the [001]-direction, the eight orientations become no longer equivalent and four of them will be flipped. Therefore, for a poled single crystal, there are four equivalent polarization directions or domains in the rhombohedral phase, namely, [111], [$\bar{1}$11], [1 $\bar{1}$1], and [$\bar{1}$ $\bar{1}$1]. The four equivalent domains are usually well aligned to form

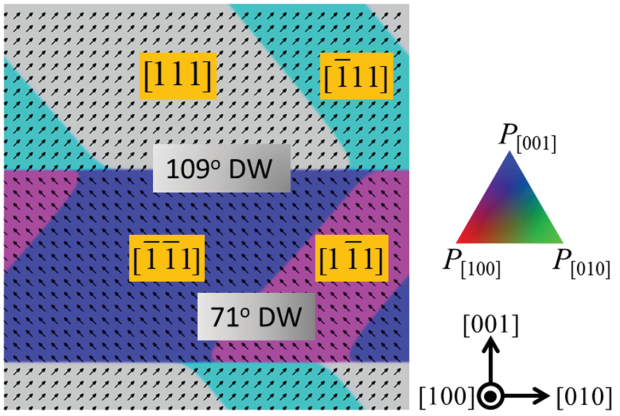

Fig. 3. (Color online) Phase-field simulated polarization distribution of the single crystal PMN–PT after electrical poling treatment along the [001]-direction. Color in RGB contours the polarization and arrows represent the in-plane projections of polarizations.

the typical "herringbone" pattern, as shown in Fig. 3. These domains are separated by either 71° or 109° domain walls. For example, the 109° domain walls can separate the [111] and [$\bar{1}$ $\bar{1}$1] domains or the [$\bar{1}$11] and [1 $\bar{1}$1] domains, while the 71° domain walls can separate the [111] and [$\bar{1}$11] domains or the [$\bar{1}$ $\bar{1}$1] and [1 $\bar{1}$1] domains, as shown in Fig. 3. If neglecting the correlations between domains, the net polarization is given by $P_r = P_s/\sqrt{3}$, where P_s is the spontaneous polarization, and such relation is confirmed by our simulation results. Therefore, the piezoelectric coefficient is no longer negligible for electrically poled ferroelectric single crystal.

In this study, the random polycrystal that consists of 16 grains with random orientations was considered. Within each grain, the polarizations have an equal probability to align along the eight ⟨111⟩ crystallographic directions for unpoled rhombohedral ferroelectric polycrystals, so the net polarization should be zero by averaging all the polarizations within a large number of grains. Upon electrical poling along the z-direction, the eight crystallographic directions become no longer equivalent, so some of the polarizations will be switched or rotated to align along the directions that are close to the z-direction. It is noted that x, y, and z in Figs. 4 and 5 are defined in the "lab coordinate". For different grain orientations, the close directions are also different. Like single crystals in Fig. 3, multiple domains and domain walls can be formed within each grain of the poled ferroelectric polycrystals. Figure 4 shows the phase-field simulated polarization distribution of PMN–PT polycrystals with random grain orientations after electrical poling treatment along the z-direction. As expected, all the polarizations are aligned along directions that are close to the z-axis and thus the net polarization P_z as well as the piezoelectric coefficient d_{33} are nonzero. If neglecting the correlation between grains, the average polarization in the poling direction is $P_z = \sqrt{3}P_s/2$ for random ferroelectric polycrystal, which was confirmed by our phase-field simulations.

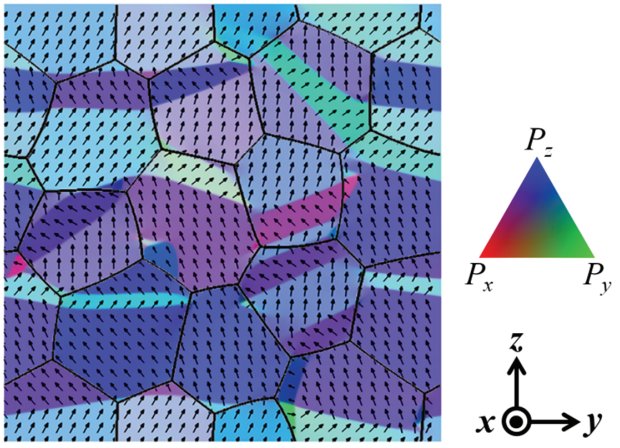

Fig. 4. (Color online) Phase-field simulated polarization distribution of PMN–PT polycrystals with random grain orientations after electrical poling treatment along the z-direction. Color in RGB contours the polarization and arrows represent the in-plane projections of polarizations. Herein, x, y, and z are defined in the "lab coordinate".

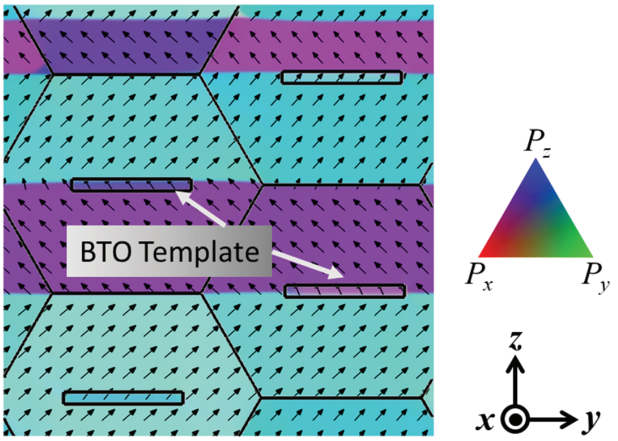

Fig. 5. (Color online) Phase-field simulated polarization distribution of PMN–PT polycrystals with [001]-textured grain orientations after electrical poling treatment along the z-direction. Color in RGB contours the polarization and arrows represent the in-plane projections of polarizations. Small rectangles represent the templates made of $BaTiO_3$.

Figure 5 shows the phase-field simulated polarization distribution of PMN–PT polycrystals with [001]-textured grain orientations after electrical poling treatment along the z-direction. Herein, z-direction coincides with the [001] crystallographic direction. In comparison with random polycrystals, the grain size of textured polycrystals is usually larger, as evident in previous experimental measurements.[15] This larger grain size is attributed to the special processing route, templated grain growth, through which the grain texture engineering is performed. The templates are made of ferroelectric $BaTiO_3$ which is in tetragonal phase at room temperature, as represented by the small rectangles in Fig. 5. Like the single crystal, upon poling along the z-direction, there are four equivalent polarization directions in the rhombohedral phase, namely, [111], [$\bar{1}$11], [1$\bar{1}$1], and [$\bar{1}\bar{1}$1]. These polarizations can be well aligned to form a "stripe" domain structure, which is in analogy to stripe domains separated by 109° domain walls in single crystals as shown in Fig. 3. In fact, such a single-crystal domain configuration appearing in textured polycrystals is attributed to the fixed [001] crystallographic axis. Nevertheless, because the other two axes are randomly distributed, correlations between neighboring grains cannot be neglected. The grain correlation results in a polarization deviation from its original direction, which eventually leads to the imperfect "stripe" domains separated by non-109° domain walls. As expected, such a single-crystal-like domain feature will not appear in random polycrystals (Fig. 4). Based on our phase-field simulation, those non-109° domain walls prefer to nucleate from the grain boundary or $BaTiO_3$ templates which, as pinning sites, will also retard the domain wall motion. If neglecting the correlations between neighboring grains, the averaged polarization of the poled textured polycrystal should be $P_z = P_s/\sqrt{3}$, the same with the single-crystal case, and the same conclusion can also be applied to the piezoelectric coefficient. The existence of grain correlation can only slightly modify the piezoelectric property if the grain size is relatively large,[26] while the templates may have a larger impact. The detailed study of the template effect on piezoelectric properties can be found in a previous work.[23]

The phase-field simulated longitudinal piezoelectric coefficients d_{33} for single crystal, random polycrystal, and [001]-textured polycrystal are shown in Fig. 6(a). As expected, the random polycrystal possesses the smallest piezoelectric coefficient due to the isotropic characteristic. The [001]-textured polycrystal fully exploits the intrinsic anisotropic properties of piezoelectric materials and thus exhibits a piezoelectric coefficient that is as large as that of single crystal. Simulation reveals that the value of d_{33} for [001]-textured polycrystal is nearly three times that of random polycrystal. To better understand the mechanism of piezoelectricity enhancement by crystallographic texturing, we obtained two energy profiles based on Landau theory. Figure 6(b) shows the Landau free energy profiles with respect to the polarization component P_z (normalized by saturated polarization P_s) along the poling direction z for random and textured polycrystals. Herein, correlations between neighboring grains or domains are excluded. The minimum-energy points correspond to the average polarization in the poling direction. For the random polycrystal, the average polarization is $P_z/P_s = \sqrt{3}/2$ (the average angle between polarization and poling direction is 30°) while for the [001]-textured polycrystal, the average polarization is $P_z/P_s = 1/\sqrt{3}$ (the average angle between polarization and poling direction is 54.74°, the maximum allowed angle for poled rhombohedral ferroelectrics). As the polarization switched from +z- to –z-direction, the textured polycrystal will experience a lower energy barrier than

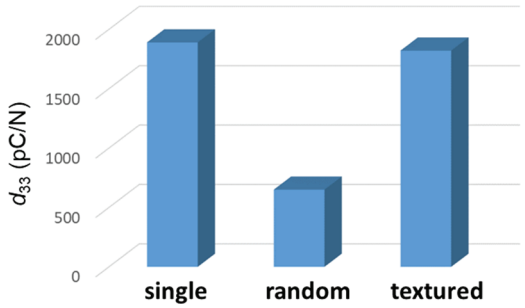

(a)

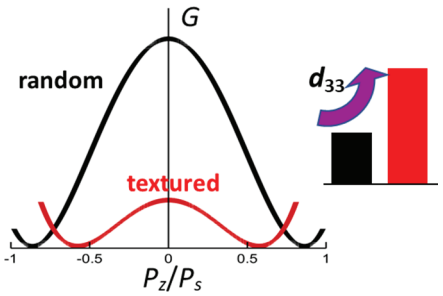

(b)

Fig. 6. (a) Phase-field simulated longitudinal piezoelectric coefficients d_{33} for single crystal, random polycrystal, and [001]-textured polycrystal. (b) Landau free energy profiles with respect to the polarization component P_z (normalized by saturated polarization P_s) along the poling direction z for random and textured polycrystals, where the inset shows the corresponding d_{33} increments.

the random polycrystal, so the textured polycrystal manifests a flatter energy landscape and thus higher ε_{33} and d_{33}.

4. Conclusion

Polycrystals with random grain orientations exhibit isotropic macroscopic properties. In order to exploit the intrinsic anisotropic properties of the materials, single crystals are desired which, however, are usually expensive or difficult to fabricate. Textured polycrystals offer better cost–performance ratio for achieving anisotropic properties. In this work, phase-field modeling and computer simulation were employed to study the effects of crystallographic textures on the piezoelectric properties of ferroelectric polycrystals at the domain level. Domain evolutions or polarization distributions for three representative microstructures, namely, single crystal, random polycrystal, and textured polycrystal, were systematically simulated. The phase-field simulations reveal that, upon electrical poling, textured polycrystal exhibits a single-crystal-like domain configuration, which does not exist in random polycrystal. The [001]-textured polycrystal fully exploits the intrinsic anisotropic properties of piezoelectric materials and thus exhibits a piezoelectric coefficient that is as large as that of single crystal, which is much larger than that of random polycrystal. To better understand the mechanism of piezoelectricity enhancement by crystallographic texturing, a theoretical analysis based on Landau theory was provided. In comparison with random polycrystal, the textured polycrystal has a flatter energy landscape and thus possesses a higher piezoelectric coefficient.

Acknowledgments

The parallel computer simulations were performed on Hefei Advanced Computing Center.

References

[1]S. J. Zhang and F. Li, High performance ferroelectric relaxor-Pb-TiO_3 single crystals: Status and perspective, *J. Appl. Phys.* **111**, 031301 (2012).
[2]K. Uchino, *Ferroelectric Devices*, 2nd edn. (CRC Press, 2009).
[3]A. Toprak and O. Tigli, Piezoelectric energy harvesting: State-of-the-art and challenges, *Appl. Phys. Rev.* **1**, 031104 (2014).
[4]E. Sun and W. Cao, Relaxor-based ferroelectric single crystals: Growth, domain engineering, characterization and applications, *Prog. Mater. Sci.* **65**, 124 (2014).
[5]U. F. Kocks, C. N. Tomé and H. R. Wenk, *Texture and Anisotropy: Preferred Orientations in Polycrystals and Their Effect on Material Properties* (Cambridge University Press, 2000).
[6]Y. K. Yan, Y. U. Wang and S. Priya, Electromechanical behavior of [001]-textured $Pb(Mg_{1/3}Nb_{2/3})O_3$-$PbTiO_3$ ceramics, *Appl. Phys. Lett.* **100**, 192905 (2012).
[7]Y. K. Yan, K. H. Cho, D. Maurya, A. Kumar, S. Kalinin, A. Khachaturyan and S. Priya, Giant energy density in [001]-textured $Pb(Mg_{1/3}Nb_{2/3})O_3$-$PbZrO_3$-$PbTiO_3$ piezoelectric ceramics, *Appl. Phys. Lett.* **102**, 042903 (2013).
[8]Y. Yan, J. E. Zhou, D. Maurya, Y. U. Wang and S. Priya, Giant piezoelectric voltage coefficient in grain-oriented modified $PbTiO_3$ material, *Nat. Commun.* **7**, 13089 (2016).
[9]Y. Saito, H. Takao, T. Tani, T. Nonoyama, K. Takatori, T. Homma, T. Nagaya and M. Nakamura, Lead-free piezoceramics, *Nature* **432**, 84 (2004).
[10]G. L. Messing, S. Trolier-McKinstry, E. M. Sabolsky, C. Duran, S. Kwon, B. Brahmaroutu, P. Park, H. Yilmaz, P. W. Rehrig, K. B. Eitel, E. Suvaci, M. Seabaugh and K. S. Oh, Templated grain growth of textured piezoelectric ceramics, *Crit. Rev. Solid State Mater. Sci.* **29**, 45 (2004).
[11]S. F. Poterala, S. Trolier-McKinstry, R. J. Meyer and G. L. Messing, Processing, texture quality, and piezoelectric properties of $\langle 001\rangle_C$ textured $(1-x)Pb(Mg_{1/3}Nb_{2/3})TiO_3$–$xPbTiO_3$ ceramics, *J. Appl. Phys.* **110**, 014105 (2011).
[12]P. Li, J. W. Zhai, B. Shen, S. J. Zhang, X. L. Li, F. Y. Zhu and X. M. Zhang, Ultrahigh piezoelectric properties in textured (K,Na)NbO_3-based lead-free ceramics, *Adv. Mater.* **30**, 1705171 (2018).
[13]Y. C. Liu, Y. F. Chang, F. Li, B. Yang, Y. Sun, J. Wu, S. T. Zhang, R. X. Wang and W. W. Cao, Exceptionally high piezoelectric coefficient and low strain hysteresis in grain-oriented (Ba, Ca)(Ti, Zr)O_3 through integrating crystallographic texture and domain engineering, *ACS Appl. Mater. Interfaces* **9**, 29863 (2017).
[14]Y. F. Chang, B. Watson, M. Fanton, R. J. Meyer and G. L. Messing, Enhanced texture evolution and piezoelectric properties in CuO-doped $Pb(In_{1/2}Nb_{1/2})O_3$-$Pb(Mg_{1/3}Nb_{2/3})O_3$-$PbTiO_3$ grain-oriented ceramics, *Appl. Phys. Lett.* **111**, 232901 (2017).
[15]Y. Yan, L. D. Geng, L.-F. Zhu, H. Leng, X. Li, H. Liu, D. Lin, K. Wang, Y. U. Wang and S. Priya, Ultrahigh piezoelectric performance through synergistic compositional and microstructural engineering, *Adv. Sci.* **9**, 2105715 (2022).

[16]W. Yang and L.-Q. Chen, Computer simulation of the dynamics of 180° ferroelectric domains, *J. Am. Ceram. Soc.* **78**, 2554 (1995).
[17]H.-L. Hu and L.-Q. Chen, Three-dimensional computer simulation of ferroelectric domain formation, *J. Am. Ceram. Soc.* **81**, 492 (1998).
[18]S. Semenovskaya and A. G. Khachaturyan, Development of ferroelectric mixed states in a random field of static defects, *J. Appl. Phys.* **83**, 5125 (1998).
[19]Y. U. Wang, Field-induced inter-ferroelectric phase transformations and domain mechanisms in high-strain piezoelectric materials: Insights from phase field modeling and simulation, *J. Mater. Sci.* **44**, 5225 (2009).
[20]A. F. Devonshire, XCVI: Theory of barium titanate, *Lond. Edinb. Dublin Philos. Mag. J. Sci.* **40**, 1040 (1949).
[21]H. Zhang, X. Lu, R. Wang, C. Wang, L. Zheng, Z. Liu, C. Yang, R. Zhang, B. Yang and W. Cao, Phase coexistence and Landau expansion parameters for a $0.70Pb(Mg_{1/3}Nb_{2/3})O_3$-$0.30PbTiO_3$ single crystal, *Phys. Rev. B* **96**, 054109 (2017).
[22]A. J. Bell, Phenomenologically derived electric field-temperature phase diagrams and piezoelectric coefficients for single crystal barium titanate under fields along different axes, *J. Appl. Phys.* **89**, 3907 (2001).
[23]J. E. Zhou, Y. Yan, S. Priya and Y. U. Wang, Computational study of textured ferroelectric polycrystals: Texture development during templated grain growth, *J. Appl. Phys.* **121**, 064108 (2017).
[24]M. E. Lines and A. M. Glass, *Principles and Applications of Ferroelectrics and Related Materials* (Clarendon Press, 1979).
[25]F. Li, S. J. Zhang, D. Damjanovic, L. Q. Chen and T. R. Shrout, Local structural heterogeneity and electromechanical responses of ferroelectrics: Learning from relaxor ferroelectrics, *Adv. Funct. Mater.* **28**, 1801504 (2018).
[26]Y. Yan, L. D. Geng, H. Liu, H. Leng, X. Li, Y. U. Wang and S. Priya, Near-ideal electromechanical coupling in textured piezoelectric ceramics, *Nat. Commun.* **13**, 3565 (2022).